Improvement of the Noise Figure of the CEBAF Switched Electrode Electronics BPM System*

Tom Powers

Thomas Jefferson National Accelerator Facility
12000 Jefferson Ave., Newport News, VA 23606

Abstract. The Continuous Electron Beam Accelerator Facility (CEBAF) is a high-intensity continuous wave electron accelerator for nuclear physics located at Thomas Jefferson National Accelerator Facility. A beam energy of 4 GeV is achieved by recirculating the electron beam five times through two anti-parallel 400 MeV linacs. In the linacs, where there is recirculated beam, the BPM specifications must be met for beam intensities between 1 and 1000 μA. In the transport lines the BPM specifications must be met for beam intensities between 100 nA and 200 μA. To avoid a complete redesign of the existing electronics, we investigated ways to improve the noise figure of the linac BPM switched-electrode electronics (SEE) so that they could be used in the transport lines. We found that the out-of-band noise contributed significantly to the overall system noise figure. This paper will focus on the source of the excessive out-of-band noise and how it was reduced. The development, commissioning and operational results of this low noise variant of the linac style SEE BPMs as well as techniques for determining the noise figure of the rf chain will also be presented.

INTRODUCTION

The switched-electrode electronics beam position monitor (SEE BPM) system, which was developed and installed in 1993–1994, was designed to operate in the CEBAF accelerator linacs where the designed beam intensity range is 1 μA to 1000 μA (1). In most of the remainder of the machine, which is collectively known as the transport lines, the nominal beam intensity range is between 100 nA and 200 μA. The exception is the Hall B transport line where beam intensities as low as 200 pA are used. Because these beam intensities are below the limits of the existing BPM systems used at CEBAF, two new systems have been developed. The system which is used at the very low-beam intensities, known as the 1 nA beam position monitoring system, is a cavity-based system which makes use of lock-in amplifiers to provide synchronous detection of the position sensitive signals. This system is fully described in (2). The second system,

* Supported by DOE Contract #DE-AC05-84ER40150

which will be described in this paper, is known as the transport line switched-electrode electronics system (TL-SEE). It is a low-noise variant of the linac style system which makes use of GaAs switches and variable gain amplifiers to cover the required dynamic range while maintaining a precise gain balance between the plus and minus signals of the X and Y electrode planes.

SYSTEM PERFORMANCE

The system performance for the linac style and transport line style SEE BPM system is summarized in Table 1. The dynamic range is defined as the range of currents for which the system operates within all other specified limits. The lower end of the dynamic range is limited by thermal noise and the detectivity of the if down-conversion circuit. The high end is limited by signal compression in the electronics.

TABLE 1. Summary of Linac Style and Transport Line Style Performance Specifications

Performance Specifications	Linac Style	Transport Line Style
Dynamic range	700 nA – 2000 μA	70 nA – 200 μA
Nominal measuring rate out of control system	1 meas./s	1 meas./s
Beam position range	$\|x\|, \|y\| \leq 5$ mm	$\|x\|, \|y\| \leq 5$ mm
Resolution (rms fluct. at nominal meas. rate)	≤ 0.1 mm	≤ 0.1 mm
Current dependence	≤ 0.1 mm	≤ 0.1 mm
Multipass capability	"snake" pulse	Not required
if bandwidth	1 MHz	50 kHz
Analog bandwidth	70 kHz	7 kHz
Maximum measurement rate	114 kS/s	7.1 kS/s

SYSTEM DESCRIPTION

Both types of SEE systems use VME based if, acquisition, and control modules. The VME crates are located in the service buildings approximately 10 meters above the beam line. Each channel consists of a BPM detector, an rf module located in the tunnel and an if module located in the VME crate. The beamline sensor has four wire-type stripline antennas previously described (3). Each pair of opposing electrodes is time-domain multiplexed into one-signal conditioning chain at the front end of the rf module (X+X–X+X–… and Y+Y–Y+Y–…). This is done to insure a balanced gain independent of gain variations in the remainder of the system. These signals are amplified and down-converted to 45 MHz before transmission to the if module. In the if module, the signal is amplified using a three-stage amplifier which has digitally controlled gain with a dynamic range of 84 dB. The signal is filtered, then down-converted to base band, filtered again and further multiplexed before it is transmitted to a commercial data acquisi-tion module as X+Y+X–Y–X+Y+… data. Each crate has a timing module which is used to synchronize the system to the accelerator and to generate specific timing signals required by the if and rf modules. The VME crate also contains three commercial data acquisition

modules and a single board microcomputer which are used to acquire and process the position signals prior to transmitting them to the machine control system.

The system has two fundamental software interfaces. The first is a once-per-second average position readout which provides the average position and its rms noise to the machine operators. The second is a beam oscilloscope program which provides time domain and frequency domain measurements of the beam position and intensity modulation at any location of the machine. Additionally, as shown in Figure 1, the program provides a measure of energy "jitter" based on beam position readings in any of five different high dispersion regions of the accelerator. The measurement shown in Figure 1 was made using five transport line BPMs whose data was acquired synchronously and processed off line using machine optics information from the CEBAF model server (4). This energy modulation was due to a problem with the phase control loop of one of the 330 superconducting cavities which are the accelerating elements at CEBAF. The problem was quickly rectified once it was identified by the BPM system.

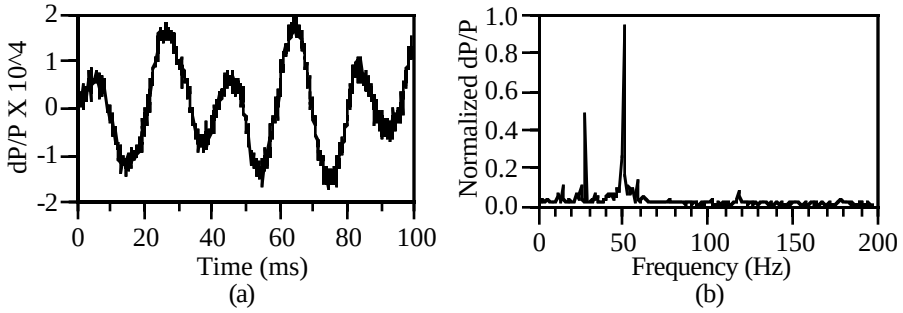

FIGURE 1. (a) Time domain and (b) frequency domain plots of the energy "jitter" in the Hall C transport line. The 50 Hz and 29 Hz frequency content was due to an SRF cavity with an open phase control loop.

BACKGROUND ON NOISE FIGURE CALCULATIONS

The noise factor of a device is the signal-to-noise ratio at the output of the device divided by the signal-to-noise ratio at the input. The noise figure is the noise factor expressed in units of dB. The noise figure is the specification that is normally provided in the component data sheet. One of the standard ways to define the noise factor (F) and noise figure (NF) is:

$$F = \frac{S_i/N_i}{S_o/N_o} = \frac{N_a + kT_oBG_a}{kT_oBG_a} \tag{1}$$

$$NF = 10 \times \log(F) \tag{2}$$

Here N_a is the noise power introduced by the device, G_a is the power gain of the device, T_o is 290 K, B is the bandwidth of the system, and k is Boltzmann's constant. Typical

noise figures for inexpensive room temperature amplifiers are 1.5 to 10 dB. Amplifiers with noise figures as low as 0.9 dB are commercially available. The noise factor of a passive two port device ($G_a < 1$), which does not contain noise sources other than thermal noise, is equal to the loss of the device, $L = 1/G_a$.

When two or more devices are cascaded, including passive devices, the noise factor for the network is given by the following equation:

$$F = F_1 + \frac{F_2 - 1}{G_1} + \frac{F_3 - 1}{G_1 G_2} + \text{L} \qquad (3)$$

Here F_1, F_2 and F_3 are the noise factors for the first, second and third stages respectively and G_1, G_2, and G_3 are the available gains of the first second and third stages respectively. Thus, once the first gain stage is accomplished the noise figure contributions to the overall noise figure by subsequent devices is reduced. This is the reason that the most important noise figure is that of the first stage amplifier and that the passive devices before the first amplifier stage should avoided if possible. However, if the front end amplifier gain is not high enough, additional losses may be such that subsequent devices may contribute significantly to the overall noise figure.

There are four contributions to the noise figure when a mixer is used as a down converter (5). The first is equal to the conversion loss of the mixer. The second is the effect of the local oscillator phase noise. The third is the noise generated by the electronic devices, (i.e., FETs for square law mixers and diodes for typical switching-mode mixers). Typically the "electronic" noise adds one or two dB to the noise figure of the circuit. The fourth contribution is the noise at the image frequency of the rf signal. Consider the signal shown in Figure 2. If there is equal noise power at the image frequency, the output noise power at the if frequency is equal to the sum of the noise power at the signal frequency plus that at the image frequency. This image frequency noise adds 3 dB to the system noise figure independent of the gain of the previous stages. In this case the noise power is added, because the two noise signals are uncorrelated.

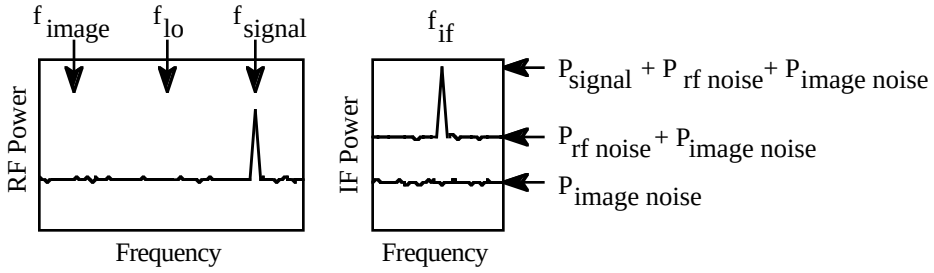

FIGURE 2. Contribution of image noise to if noise at the output of a mixer.

Measurement Techniques

There are several ways to measure the noise figure of a device or system. The first is to plot the output noise power with a 50 ohm source impedance at different temperatures (typically 300 K and 77 K)(6). The P-intercept of a straight-line plot of measured output

power as a function of temperature is the value of the noise power N_a of the device under test. The second approach is to use a calibrated noise source, a low-noise amplifier (LNA) and noise figure meter, or spectrum analyzer with a noise figure personality module. In this technique, the spectral characteristics of the noise source and LNA are measured, the device under test (DUT) is inserted between them, and the instrument calculates the gain and noise figure of the DUT. The third method requires an LNA, a spectrum analyzer and a 50 ohm termination. In the latter two techniques the LNA is used to increase the sensitivity of the measuring instrument in order to increase the measured noise voltage above the noise floor of the instrument. The last technique has the added advantage that "man-made" signal sources become apparent when the measurement is being made and one may make compensations, while the first two systems provide only a noise figure at specific frequencies.

The noise factor of an amplifier can also be written as:

$$F = \frac{P}{kTBG} \tag{4}$$

Here P is the output noise power with the input terminated, T is the absolute temperature of the termination, k is Boltzmann's constant, and G is the amplifier gain. For a 50 ohm system with a preamplifier inserted between the DUT and the spectrum analyzer this equation may be written as:

$$NF(\text{dB}) = 10 \log \frac{V^2}{R} - 10 \log B - 10 \log (G_a + G_p) - 10 \log kT \tag{5}$$

Here G_p is the gain of the preamplifier, V is the rms voltage reading, and B is the measurement bandwidth. The reading is done using the voltage scale in order to increase the resolution. This equation can be further reduced to:

$$NF(\text{dB}) = 20 \log V - 10 \log BW - 10 \log (G_a + G_p) - 187.27 \text{ dB} \tag{6}$$

Here BW is the 3 dB bandwidth of the spectrum analyzer, and 187.27 is a result of the sum of four numbers: –10 log 50 ohms, –10 log kT, –10 log 1.2 (an approximate correction factor to go from noise power bandwidth to Gaussian 3 dB bandwidth), and +1.05 dB (detector correction factor) (7). In order to make accurate voltage measurements, strong video averaging is applied with typical averaging factors of 1000. Additionally, one must be careful to keep the peak signals, without averaging, below the saturation levels of the instrument by adjusting the vertical scale with averaging off and turning averaging on before making a measurement.

IMPROVEMENT TO THE NOISE CHARACTERISTICS

Four fundamental changes were made to the system to improve the low current operations. Three changes were made to the rf module which improved the noise characteristics at lower beam intensity by 8 dB or a factor of 2.5. Improvements were made to the if module which increased the sensitivity by 13 dB, or an additional factor of 4.4 lower in beam intensity. These improvements should have extended the dynamic

range at low currents by a factor of 11, from 700 nA to 64 nA. As will be shown, the actual increase in sensitivity was only a factor of 10, or down to 70 nA.

Intermediate Frequency Module Improvements

The function of the if module is to amplify the if signal provided by the rf module and down-convert it to a baseband signal that can be digitized with a commercial ADC module. A simple schematic diagram of the linac style if module is shown in Figure 3. A detailed description of the function of the linac style if module may be found in (1). Three changes were made to improve the noise characteristics of the system: the 1 MHz BW at 45 MHz LC filter was changed to a 50 kHz BW at 45 MHz crystal filter; the 860 kHz low-pass filter was changed to a 100 kHz low-pass filter; and the integration time of the gated integrated filter was changed from 3.2 μs to 30 μs. This last change was done because the switching clock frequency was reduced from 248 kHz to 14.2 kHz so that the plus-to-minus modulated if signal has settled sufficiently before the integration process is initiated. The settling time for the 1 MHz BW filter is 500 ns while the settling time of the 50 kHz BW filter is 25 μs. The changes which were made to the baseband section of the if module improved the noise characteristics of the output signal, while the low-current limitation of the system remained the ability of the video detector to lock on the if frequency in the presence of noise. Thus the only improvement which impacted the low-current limit was the reduction of the bandwidth of the 45 MHz band pass filter.

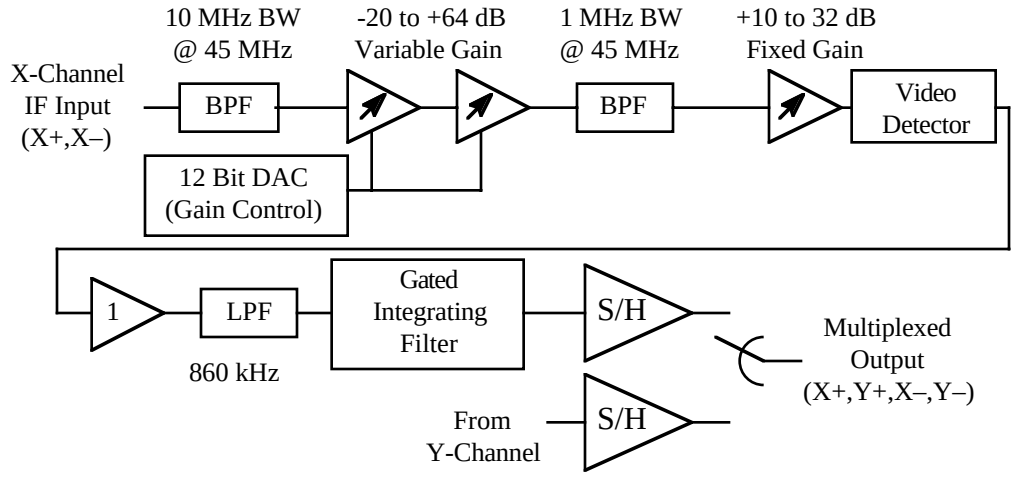

FIGURE 3. Simplified schematic diagram of the linac style if module.

Radio-Frequency Module Improvements

A detailed functional description of the rf module can be found in (1). The rf chains for the two systems are shown in Figure 4. Three changes were made to the linac-style system in order to improve the low-current performance. The first change is that the 1497 MHz band pass filter was relocated to just before the mixer in order to improve the

overall noise figure by 6.8 dB. For the second change, the two-stage rf amplifier was changed from two MAR-6 amplifiers to one MAR-6 amplifier and one ERA-3 amplifier. This increased the rf gain from 23 dB to 32 dB without degrading the noise figure. Thirdly, the gain was adjusted on the output stage if amplifier to provide an overall gain of 38 dB in contrast with the 25 dB setting used in the linac style system. This, along with increased overall gain prior to this section, had the additional benefit of decreasing the overall noise figure by another 1.5 dB. The range of input power levels for the linac style rf module is –77 dBm to –4 dBm, which equates to an intensity range of 700 nA to 2 mA. The range of inputs for the transferline-style rf module is –97 dBm to –27 dBm, which equates to an intensity range of 70 nA to 200 μA.

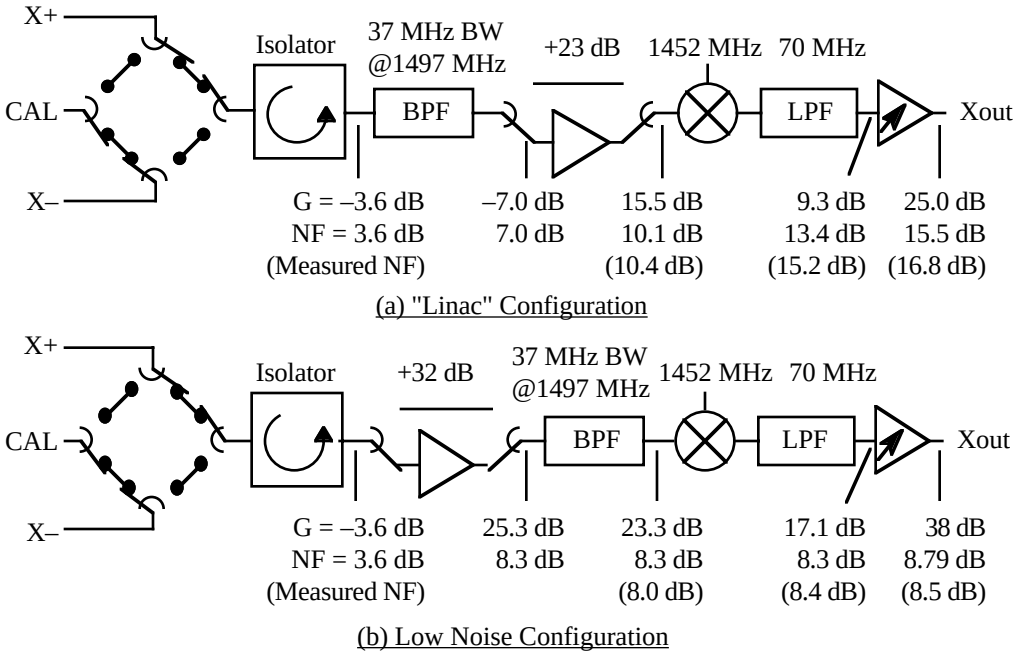

FIGURE 4. Switched-electrode electronics rf chain schematic diagrams showing the linac configuration and the low-noise, transport line, configuration. The noise figures within parentheses are measured values while the other noise figures, as well as the gains (G), were calculated based on typical measured values.

Relocating the filter had two expected and one unexpected effects. The first effect is the reduction of the overall noise figure by 2 dB (the in-band attenuation of the filter) because the filter was moved to a point after the initial gain stage. Thus the contribution to the noise figure due to the loss was reduced by $(F_{filter}-1)/G_i$ where G_i is the combined gain of the switches, the circulator and the two-stage amplifier. The second effect was the reduction of the overall noise figure by 3 dB because the filter rejected the noise at the image frequency of 1542 MHz. The third effect was one of the two more subtle improvements associated with the changes.

When performing the initial system noise figure measurements, the circuit, at the mixer output, had 2 dB of unaccounted-for noise figure. Figure 5 shows the normalized noise power as a function of frequency at the input of the mixer for both circuits. The noise power at the image frequency for the circuit with the filter prior to the amplifier is

1.8 times the power level at the signal frequency. By adding this to the in-band noise you would get a noise figure increase of 5 dB as opposed to the 3 dB that is expected from an SSB down conversion with uniform noise in both the image and signal frequency bands. Further investigation of the characteristics of the band pass filter indicated that the filter does reject signals at the image frequency by more than 30 dB. However, the output port of the filter is almost totally reflective at the image frequency. A reflective source will reflect any noise power coming out of the input port of the amplifier circuit back into the amplifier for amplification. The second subtlety is the noise figure of the AD603 variable gain amplifier, which is the last stage of the circuits shown in Figure 4. The first page of the specification sheet indicates that the input noise spectral density is 1.3 $nV/Hz^{1/2}$, which corresponds to a noise figure of 9.5 dB for the amplifier bandwidth of 50 MHz and a gain of 32 dB. However, the variable gain function of this amplifier was implemented by an R-2R ladder network followed by a fixed-gain amplifier. This ladder network is, in effect, a voltage-controlled attenuator. Thus, as the overall gain is reduced by 10 dB, the noise figure of the AD603 increases by 10 dB. By increasing the gain of the if stage from 18 dB to 23 dB, the noise figure of the if stage was reduced from 21 dB to 16 dB and the overall noise figure of the rf module was reduced by 0.85 dB.

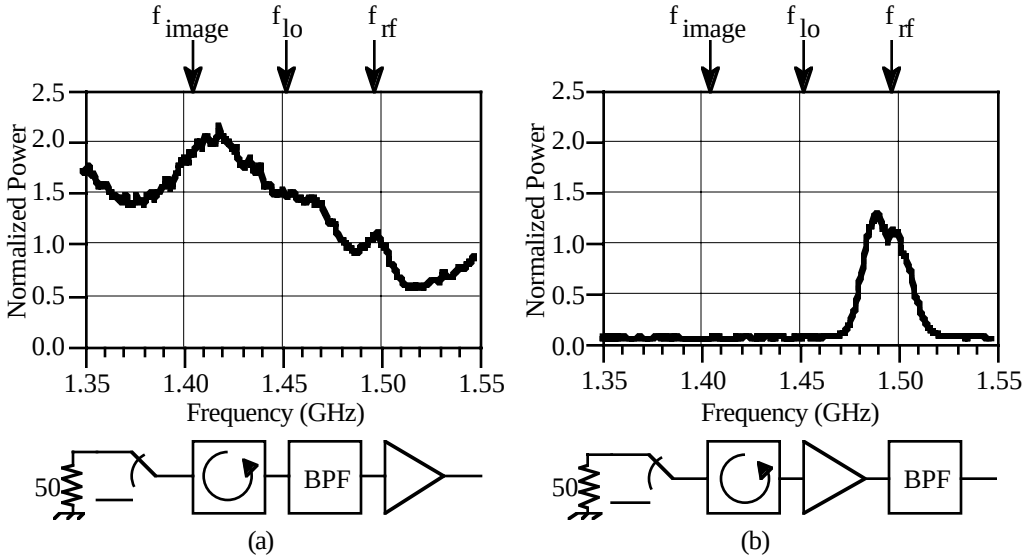

FIGURE 5. Normalized noise power as a function of frequency for two different circuit topologies. The first is the topology used in the linac style system while the second is that used in the transport line system.

RESULTS

During the production testing the low-current capability of all of the rf modules was determined. For practical reasons, this low-current limit is defined by the rms value of the position noise. As is shown in Figure 6, the low-current beam position is valid (within 200 μm of the maximum value) when the rms value of the instantaneous beam position readings is less than 1 mm. Further analysis of the production test data shows that position readings at the minimum current value on all of the channels used to

generate Figure 6(b) were within +/– 120 μm of the maximum value. An additional 12% reduction in beam current was required before any of the modules varied by more than 200 μm from the maximum position. Figure 7 shows histograms of the results of this analysis. Only two of the transport line modules that were analyzed had a measured low current limit above 70 nA while most of the modules made it down to 60 nA. This data is shown in Figure 7(b). An analysis of the production data from the linac style modules indicates that the low-current limit for this style is 700 nA with most modules making it down to 550 nA. This data is shown in Figure 7(a).

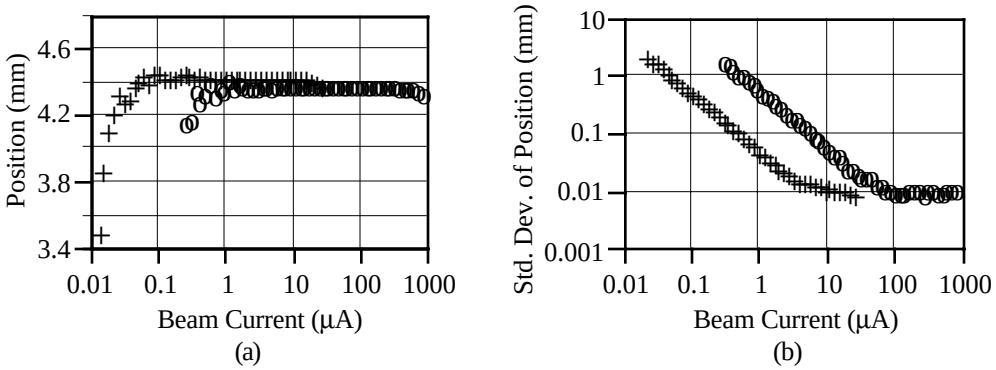

FIGURE 6. Typical plots of (a) beam position as a function of beam intensity and (b) standard deviation of the 140 μs beam position readings as a function of beam intensity. Both sets of data were taken using transport style electronics in the laboratory. The data indicated with a "+" is for the high gain setting and an "o" is for the low gain setting.

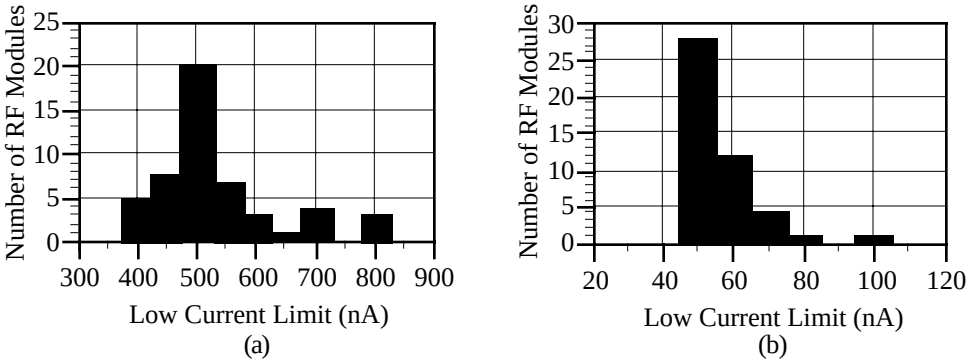

FIGURE 7. Low current limitations of (a) 48 linac-style rf modules and (b) 46 transport line rf modules as measured during production testing.

CONCLUSION

A description of how the noise figure is measured as well as the basic formula for calculation of the noise figure of a multi-stage system have been presented. Application of these principles to improve the low current operation of the SEE BPM system was also described. By changing the bandwidth of the if section, the judicious swapping of

circuit elements in the rf section, and the adjustment of the gains in the rf module, the low-current capabilities have been improved from 700 nA to below 70 nA. This was accomplished without doing a major redesign of the system packaging, digital interface, or software.

REFERENCES

[1] Powers, T., et al., "Design, Commissioning and Operational Results of Wide Dynamic Range BPM Switched Electronics," *Proceedings of the Seventh Beam Instrumentation Workshop*, p 257.

[2] Piller, C., et. al, "1 nA Beam Position Monitor," presented at this conference.

[3] Barry, W., *Nucl Instrum Meth A*, **301**, pp. 407–416, 1991.

[4] Van Zeijts, J., et al., "Integrated On-Line Accelerator Modeling at CEBAF", *Proceedings of the 1995 Particle Accelerator Conference*, p. 2181.

[5] Hayward, W., *Introduction to Radio Frequency Design*, American Radio Relay League, Inc. 1994, pp. 202–246.

[6] Gardiol, F. E., *Introduction to Microwaves*, Artech House, Inc. 1984, p. 362

[7] "Spectrum Analysis, . . . Noise Analysis" Hewlett Packard Application note 150–4, April 1974.